

Planar Near-Field Antenna Measurements Using Nonideal Measurement Locations*

R. C. Wittmann, B. K. Alpert, and M. H. Francis
National Institute of Standards and Technology
325 Broadway, Boulder, CO 80303-3328

Abstract— The standard planar near-field to far-field transformation method requires data points on a plane-rectangular lattice. In this paper we introduce a transformation algorithm in which measurements are neither required to lie on a regular grid nor are strictly confined to a plane. Computational complexity is $\mathcal{O}(N \log N)$, where N is number of data points. (Actual calculation times depend on the numerical precision specified and on the condition number of the problem.) This algorithm allows efficient processing of near-field data with known probe position errors. Also, the algorithm is applicable for other measurement approaches, such as plane-polar scanning, where data are collected on a nonrectangular grid.

Keywords: near-field antenna measurements; planar scanning; plane-polar scanning; probe position errors

1. INTRODUCTION

The standard planar near-field antenna measurement technique requires that data be obtained on a plane-rectangular grid. However, it is not always practical or desirable to make regularly spaced measurements. The maintenance of positioning tolerances becomes more difficult as frequency is increased. An efficient algorithm for processing data with probe position errors can significantly extend the frequency ranges of existing scanners. Such an algorithm can also make it practical to consider portable scanners for on-site antenna measurements. In addition, there has been much recent interest in schemes, such as plane-polar scanning, where data are collected on a nonrectangular grid.

Here we introduce an algorithm which does not require “ideal” probe locations. We do assume, however, that the probe positions are known. (In practice, laser interferometry is often used for this purpose.) Our approach is based on combining the recently developed unequally spaced fast Fourier transform [1], interpolation, and the conjugate gradient algorithm. Computational complexity is $\mathcal{O}(N \log N)$

operations per iteration, where N is the number of measurements. The number of iterations depends on desired computational accuracy and on conditioning (see below). We present several simulations, which are based on actual antenna data.

2. THE MODEL

Consider a transmitting test antenna (located in the half space $z < 0$) and a receiving probe (translated without rotation). According to Kerns’s theory [2], the probe response $w(\mathbf{r})$ may be modeled as

$$w(\mathbf{r}) = \sum_{\nu\mu} \xi_{\nu\mu} \exp(i\mathbf{k}_{\nu\mu} \cdot \mathbf{r}), \quad z > 0 \quad (1)$$

[$\exp(-i\omega t)$ time convention], where $\xi_{\nu\mu}$ is the (normalized) coupling product and

$$\begin{aligned} \mathbf{k}_{\nu\mu} &\equiv \frac{\pi\nu}{L_x} \hat{\mathbf{x}} + \frac{\pi\mu}{L_y} \hat{\mathbf{y}} + \gamma_{\nu\mu} \hat{\mathbf{z}} \\ \gamma_{\nu\mu} &\equiv \sqrt{k^2 - \left(\frac{\pi\nu}{L_x}\right)^2 - \left(\frac{\pi\mu}{L_y}\right)^2} \\ k &\equiv \omega/c. \end{aligned}$$

We assume that the probe response is negligible outside the interval $|x| \leq L_x$, $|y| \leq L_y$ for z values of interest. [That is, $w(\mathbf{r})$ is a periodic extension.] To improve conditioning (see below), we include only propagating plane waves ($\gamma_{\nu\mu}$ real) in the summation in (1). Evanescent waves ($\gamma_{\nu\mu}$ imaginary) are exponentially attenuated and are negligible in the far-field region. We must also ensure that evanescent waves are not important contributors to the measured probe response; this is usually accomplished by maintaining a probe-to-test-antenna separation of several wavelengths.

In matrix form (1) becomes

$$\mathbf{w} = \mathbf{Q}\boldsymbol{\xi} \quad (2)$$

where $\mathbf{w} \equiv \{w(\mathbf{r}_n)\}$, \mathbf{r}_n is the location of the n th measurement point, $\boldsymbol{\xi} \equiv \{\xi_{\nu\mu}\}$, and

*U.S. Government contribution not subject to copyright in the United States.

$\mathbf{Q} \equiv \{Q_{n,\nu\mu} = \exp(i\mathbf{k}_{\nu\mu} \cdot \mathbf{r}_n)\}$. The objective of near-field to far-field transformation is to determine the coupling product $\boldsymbol{\xi}$ from measurements \mathbf{w} made in a restricted region near the test antenna. The transmitting (far-field) pattern can be found from the coupling products of the test antenna with each of two independent, known probes.

3. NORMAL EQUATIONS

In practical situations, where the number of measurements often exceeds the number of unknowns, the system (2) is overdetermined and will generally not have a solution. We will actually solve the normal equations

$$\mathbf{A}\boldsymbol{\xi} = \mathbf{b}, \quad (3)$$

where

$$\begin{aligned} \mathbf{A} &\equiv \mathbf{Q}^H \mathbf{Q} \\ \mathbf{b} &\equiv \mathbf{Q}^H \mathbf{w}. \end{aligned}$$

The operator $\mathbf{Q}^H \equiv \{Q_{\nu\mu,n}^H = \exp(-i\mathbf{k}_{\nu\mu}^* \cdot \mathbf{r}_n)\}$ is the Hermitian (conjugate) transpose of \mathbf{Q} . The solution $\boldsymbol{\xi}$ of (3) minimizes $\|\mathbf{w} - \mathbf{Q}\boldsymbol{\xi}\|$; that is, this $\boldsymbol{\xi}$ is the least-squares estimate. Most methods for processing planar near-field data [based on the model (1)] solve (3), either directly or indirectly. In the standard plane-rectangular grid algorithm, \mathbf{A} is diagonal and \mathbf{Q}^H and \mathbf{Q} can be applied with fast Fourier transforms, giving a computational complexity of $\mathcal{O}(N \log N)$. On the other hand, a direct solution using Gaussian elimination requires $\mathcal{O}(N^3)$ operations. For typical problem sizes ($10^4 < N < 10^6$), the importance of computational efficiency is readily apparent.

4. CONJUGATE GRADIENT SOLUTION

Because \mathbf{A} is Hermitian and positive definite (assuming that \mathbf{Q} is full rank), any of a number of conjugate gradient algorithms [3] is applicable. We implement the iterative scheme

$$\begin{aligned} \mathbf{d}^{(0)} &= \mathbf{r}^{(0)} = \mathbf{b} - \mathbf{A}\boldsymbol{\xi}^{(0)} \\ \alpha_j &= \frac{\|\mathbf{r}^{(j)}\|^2}{[\mathbf{d}^{(j)}]^H \mathbf{A} \mathbf{d}^{(j)}} \\ \boldsymbol{\xi}^{(j+1)} &= \boldsymbol{\xi}^{(j)} + \alpha_j \mathbf{d}^{(j)} \\ \mathbf{r}^{(j+1)} &= \mathbf{r}^{(j)} - \alpha_j \mathbf{A} \mathbf{d}^{(j)} \\ \mathbf{d}^{(j+1)} &= \mathbf{r}^{(j+1)} + \frac{\|\mathbf{r}^{(j+1)}\|^2}{\|\mathbf{r}^{(j)}\|^2} \mathbf{d}^{(j)}, \end{aligned} \quad (4)$$

where $\|\mathbf{y}\|^2 \equiv \mathbf{y}^H \mathbf{y}$. Initial estimates are not critical and we use $\boldsymbol{\xi}^{(0)} = 0$ for simplicity. Somewhat earlier convergence may be obtained, for example, by starting with the coupling product obtained from k -corrected data [4]. The quantity $\mathbf{r}^{(j)} = \mathbf{b} - \mathbf{A}\boldsymbol{\xi}^{(j)}$ is the j th residual.

Rate of convergence can be estimated with [5, p. 525]

$$\|\boldsymbol{\xi}^{(j)} - \boldsymbol{\xi}\|_A \leq 2 \left(\frac{c-1}{c+1} \right)^j \|\boldsymbol{\xi}^{(0)} - \boldsymbol{\xi}\|_A, \quad (5)$$

where $\|\mathbf{y}\|_A^2 \equiv \mathbf{y}^H \mathbf{A} \mathbf{y}$ and the condition number c^2 is the ratio of the largest to smallest eigenvalue of \mathbf{A} . (The condition number of \mathbf{Q} is c , $c \geq 1$.) Thus, *the conjugate gradient algorithm will always converge.*

5. CONDITIONING

Relative error is bounded by the residual

$$\frac{\|\boldsymbol{\xi}^{(j)} - \boldsymbol{\xi}\|}{\|\boldsymbol{\xi}\|} \leq c^2 \frac{\|\mathbf{r}^{(j)}\|}{\|\mathbf{b}\|}. \quad (6)$$

If we suppose that “perfect” measurements \mathbf{w}_0 and “imperfect” measurements \mathbf{w} correspond to the solutions [of (3)] $\boldsymbol{\xi}_0$ and $\boldsymbol{\xi}$, then

$$\frac{\|\boldsymbol{\xi} - \boldsymbol{\xi}_0\|}{\|\boldsymbol{\xi}_0\|} \leq c \frac{\|\mathbf{w} - \mathbf{w}_0\|}{\|\mathbf{w}_0\|}. \quad (7)$$

When condition numbers are large (poor conditioning), equations (5)–(7) indicate *potential problems* with convergence rate, computational accuracy, and/or experimental design. Fortunately, it is often possible to improve conditioning by adding physically reasonable restrictions. For example, arbitrarily large condition numbers can arise when evanescent plane waves are included in the model (1). In the examples of section 7, the exclusion of evanescent fields results in reasonable condition numbers.

6. EFFICIENCY

In the conjugate gradient procedure of equations (4), it is necessary to apply the matrix $\mathbf{A} = \mathbf{Q}^H \mathbf{Q}$ to a vector once each iteration. This can be done by a straightforward summation, but only in $\mathcal{O}(N^2)$ operations. In order to reduce complexity to $\mathcal{O}(N \log N)$ operations per iteration, we have developed a scheme that combines the unequally spaced fast Fourier transform with interpolation in z . For example, to apply \mathbf{Q} to $\boldsymbol{\xi}^{(j)}$, we use the unequally spaced fast Fourier transform to evaluate (2) [in $\mathcal{O}(N \log N)$ operations] at the points (x_n, y_n, z) for several fixed values of z . We then use local interpolation in z to reach

the actual measurement locations \mathbf{r}_n . Computational time depends on the desired numerical accuracy and on the spatial distribution of data points. Since we are dealing with bandlimited functions, the numerical precision of the algorithm can be controlled and is specified as an input parameter. Our technique is most efficient when measurement locations lie close to a plane. Details will be presented elsewhere.

7. SIMULATIONS

7.1 Probe position errors

We began with planar near-field data for a radiometer antenna with an aperture diameter of 25 cm and an operating frequency of 31.65 GHz. These data consist of 161 points in x by 161 points in y spaced by 0.38 cm (0.4λ). The model (1) was specified with $L_x = L_y = 161 \times 0.38/2 = 30.59$ cm and the coupling product was calculated using standard near-field to far-field transformation software. Position errors were then simulated by using (1) to calculate the probe response at nonideal measurement locations. In this setup, there are about 26 000 simulated measurements and about 20 000 unknowns (evanescent modes excluded). We considered three cases:

For the first case, we used a moderate position error of the form:

$$\begin{pmatrix} \Delta x \\ \Delta y \\ \Delta z \end{pmatrix} = \begin{pmatrix} 0.14 \cos(0.35n) \cos(0.65m) \\ 0.14 \cos(0.25n) \cos(0.15m) \\ 0.20 \cos(0.15n) \cos(0.11m) \end{pmatrix} \lambda, \quad (8)$$

where n is the x index and m is the y index. Both indices run from -80 to $+80$. Peak magnitude of this position error is 0.28λ and the rms magnitude is 0.14λ . Figure 1 shows the result of probe position correction in this example. There is no discernible difference between actual and position corrected patterns. However, the pattern computed ignoring probe position errors has a broader main beam than the correct pattern and also has a gain that is about 2 dB too low. The relative residual at the j th iteration is defined as

$$\tau_j \equiv \left\| \mathbf{r}^{(j)} \right\| / \left\| \mathbf{b} \right\|.$$

We terminate our program after j_{max} iterations or after the relative residual becomes less than τ (say, $j_{max} = 100$ and $\tau = 10^{-8}$). For the displacements (8), the condition number is $c^2 = 12.8$, $\tau_5 < 10^{-4}$, and $\tau_{19} < 10^{-8}$. Condition numbers are estimated using a procedure due to Lanczos [5, p. 523]. Calculations were done on a high performance RISC work station and required approximately 1 minute per iteration.

The second case was a more severe test:

$$\begin{pmatrix} \Delta x \\ \Delta y \\ \Delta z \end{pmatrix} = \begin{pmatrix} 0.3 \cos(0.35n) \cos(0.65m) \\ 0.3 \cos(0.25n) \cos(0.15m) \\ 1.0 \cos(0.15n) \cos(0.11m) \end{pmatrix} \lambda. \quad (9)$$

The peak magnitude of this position error is 1.1λ and the rms magnitude is 0.52λ . Figure 2 shows the result of probe position correction in this example. The pattern computed ignoring probe position errors bears little resemblance to the correct pattern—even the main beam is no longer recognizable. Again, there is no discernible difference between actual and position corrected patterns. For the displacements (9), the condition number is $c^2 = 21$, $\tau_9 < 10^{-4}$, and $\tau_{29} < 10^{-8}$.

The third case used the position errors of the second case [see (9)], but a phase gradient was introduced into the near-field data to steer the main beam 30° from boresight. As shown in figure 3 the pattern, ignoring probe position errors, bears little resemblance to the correct pattern. If we correct only for z position errors, much of the true pattern is recovered. However, the gain is still about 1 dB too low, and there are some anomalous sidelobes. The condition number and the number of iterations were the same as in the second case. This example demonstrates the importance of 3 dimensional position error correction for steered beam antennas.

7.2 Plane-polar grid

Beginning with the model and the coupling product data used in section 7.1, we simulated probe response on a plane-polar grid: maximum radius $r_{max} = 43$ cm; radial step $\Delta r = 0.4\lambda$; angular step $\Delta\phi = \pi/356$ (so that $r_{max}\Delta\phi = 0.4\lambda$). Data were retained within the rectangle $|x|, |y| < 30.59$ cm. In this setup, there are about 65 000 simulated measurements. A direct application of our algorithm resulted in a poor condition number $c^2 \approx 2\,400$ and $\tau_{100} \approx 5 \times 10^{-7}$.

The condition number can be dramatically reduced by finding a weighted least-squares solution of (2). For example, when data points were weighted by their measurement radii, the condition number was $c^2 = 46$, and $\tau_{29} < 10^{-8}$. This weighting scheme is consistent with an “information content” that is constant per unit area.

Alternately, by simply thinning the data so that measurement spacing was never less than 0.15 cm, the condition number was reduced to $c^2 = 5.9$ and $\tau_{17} < 10^{-8}$. (In this setup, the number of simulated measurements is about 44 000.)

There are noniterative schemes for processing plane-polar data in $\mathcal{O}(N \log N)$ operations [6]–[8].

Our approach is more flexible, however, since data locations can be perturbed in 3 dimensions.

8. SUMMARY

A number of papers that treat nonideal measurement locations have been published [9]–[11]. We think that our approach compares favorably in terms of efficiency, accuracy, and simplicity. Major features are:

- The algorithm is iterative, with a fixed cost per iteration that is $\mathcal{O}(N \log N)$. The memory requirement is $\mathcal{O}(N)$ and is independent of the number of iterations.
- Convergence is guaranteed. Bounds [see (5)] on the convergence rate for the conjugate gradient procedure are tighter than for many alternative iterative techniques.
- Computation error (not measurement error, of course) is bounded by the residual [see (6)].
- Our current implementation is fully 3 dimensional.
- The recipe given in this paper is also applicable to cylindrical and spherical scanning geometries. The basic ingredient is an efficient procedure for predicting probe response at the measurement locations, based on an estimated modal spectrum.

REFERENCES

- [1] G. Beylkin, “On the fast Fourier transform of functions with singularities,” *Applied and Computational Harmonic Analysis*, vol. 2, pp. 363–381, 1995.
- [2] D. M. Kerns, “Plane-wave scattering-matrix theory of antennas and antenna-antenna interaction,” Nat. Bur. Stand. (U. S.) Monograph 162, 1981.
- [3] R. E. Kleinman and P. M. van den Berg, “Iterative methods for solving integral equations,” ch. 3 in *PIER 5. Application of Conjugate Gradient Method to Electromagnetics and Signal Analysis*, ed. T. K. Sarkar. New York: Elsevier, 1991.
- [4] E. B. Joy, and R. E. Wilson, “A simplified technique for probe position error compensation in planar surface near-field measurements,” *Proc. Antenna Measurement Techniques Assoc.*, pp. 14-1 to 14-10, Oct. 1982.
- [5] G. H. Golub and C. F. Van Loan, *Matrix Computations*. Baltimore: Johns Hopkins, 1989.
- [6] O. M. Bucci, C. Gennarelli, and C. Savarese, “Fast and accurate near-field—far-field transformation by sampling interpolation of plane-polar measurements,” *IEEE Trans. Antennas Propagat.*, vol. AP-39, pp. 48–55, Jan. 1991.
- [7] L. I. Williams, Y. Rahmat-Samii, and R. G. Yaccarino, “A comparison of polar, thinned-polar, and linear spiral sampling using the UCLA bipolar planar near-field measurement system,” *Proc. Antenna Measurement Tech. Assoc.*, pp. 358–363, Nov. 13–17, 1995.
- [8] A. D. Yaghjian and M. B. Woodworth, “Sampling in plane-polar coordinates,” *IEEE Trans. Antennas Propagat.*, vol. AP-44, pp. 696–700, May 1996.
- [9] L. E. Corey and E. B. Joy, “On computation of electromagnetic fields on planar surfaces from fields on nearby surfaces,” *IEEE Trans. Antennas Propagat.*, vol. AP-29, pp. 402–404, March 1981.
- [10] P. K. Agrawal, “A method to compensate for probe positioning errors in an antenna near-field facility,” *Proc. IEEE Antennas Propagat. Int. Symp.*, Albuquerque, NM, pp. 218–221, July 1982.
- [11] L. A. Muth, “General order N analytic correction of probe-position errors in planar near-field measurements,” *Proc. Antenna Measurement Tech. Assoc.*, pp. 331–335, Nov. 13–17, 1995.

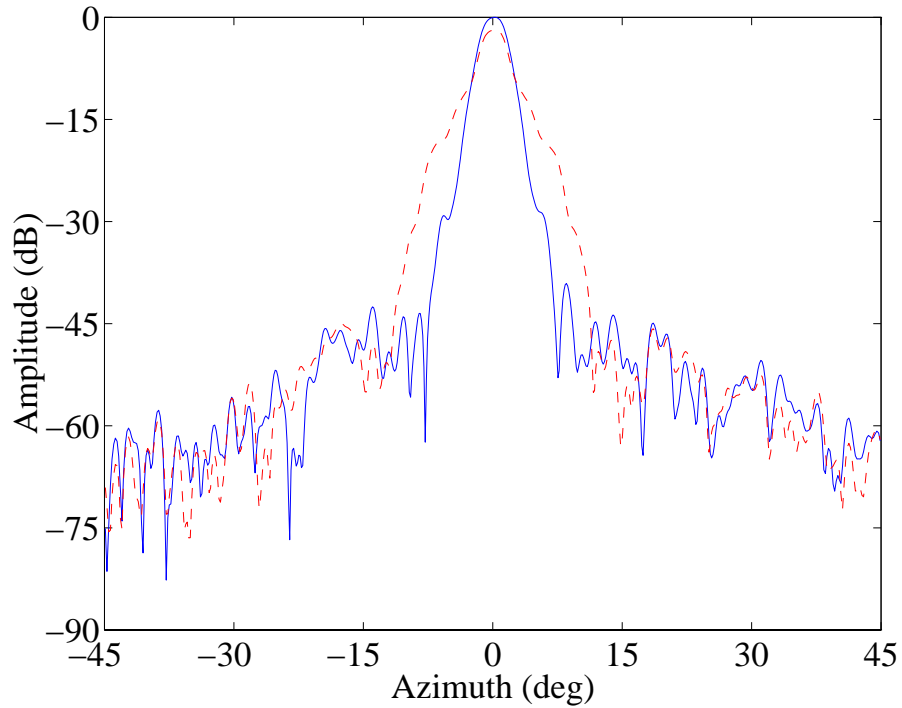


Figure 1 – H-plane far-field pattern of the test antenna. Probe position errors are given by eq (8). The solid line corresponds to the corrected pattern and to the actual pattern. The dashed line shows the result of ignoring the position errors.

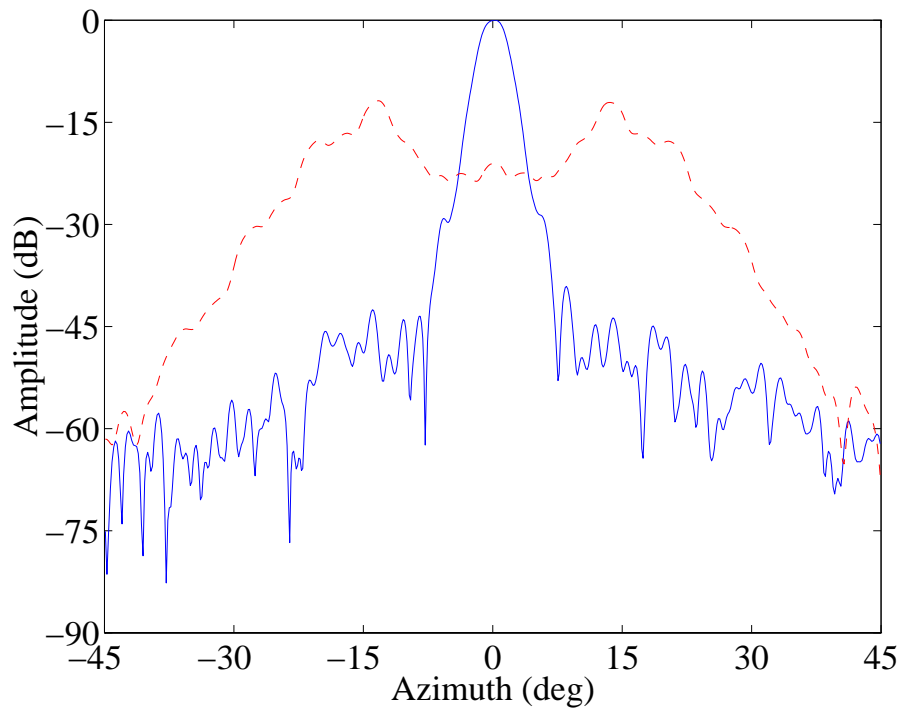


Figure 2 – H-plane far-field pattern of the test antenna. Probe position errors are given by eq (9). The solid line corresponds to the corrected pattern and to the actual pattern. The dashed line shows the result of ignoring the position errors.

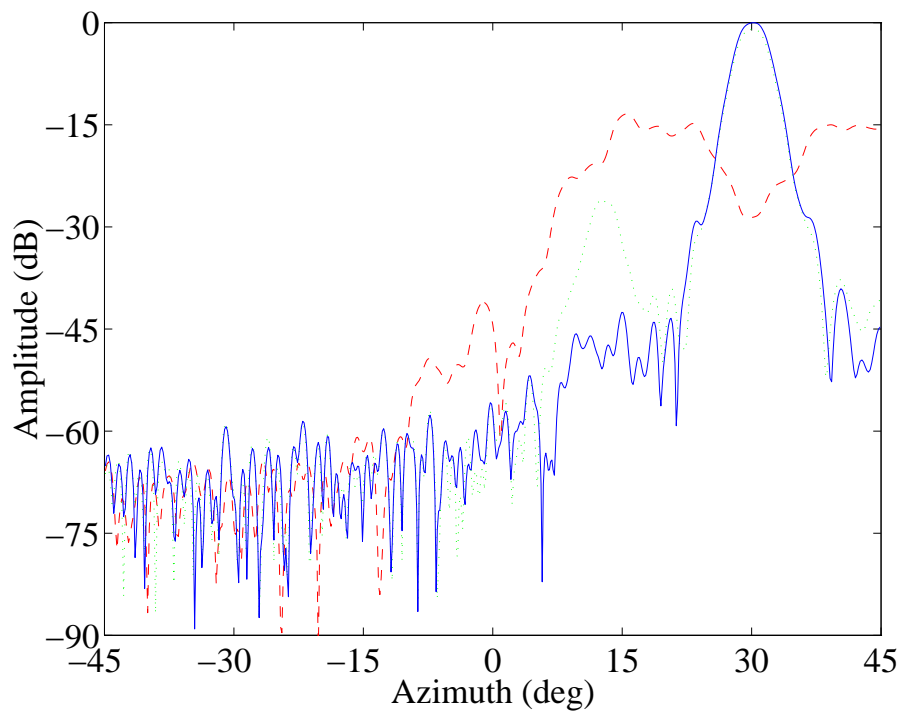


Figure 3 – H-plane far-field pattern of the antenna with a steered beam. Probe position errors are given by eq (9). The solid line corresponds to the corrected pattern and to the actual pattern. The dashed line shows the result of ignoring the position errors. The dotted line is the result of correcting for only the z position errors.